Sublithographic vertical gold nanogap for label-free electrical detection of protein-ligand binding

Dong-Yoon Jang[a)]
Department of Electrical Engineering and Computer Sciences, KAIST, 373-1 Guseong-Dong, Yuseong-Gu, Daejeon 305-701, Korea

Young-Pil Kim and Hak-Sung Kim
Department of Biological Sciences, KAIST, 373-1 Guseong-Dong, Yuseong-Gu, Daejeon 305-701, Korea

Sang-Hee Ko Park and Sung-Yool Choi
Electronics and Telecommunications Research Institute (ETRI), 161 Gajeong-Dong, Yuseong-Gu, Daejeon 305-700, Korea

Yang-Kyu Choi
Department of Electrical Engineering and Computer Sciences, KAIST, 373-1 Guseong-Dong, Yuseong-Gu, Daejeon 305-701, Korea

Label-free electrical detection of protein-ligand binding using a vertical gold nanogap is presented. A sublithographic nanogap was created using a sacrificial ultrathin film deposited by atomic layer deposition (ALD) in a process similar to the formation of a cantilever in microelectromechanical system processing. Due to the atomic precision of the sacrificial Al_2O_3 thickness by ALD, a 7 nm nanogap was successfully fabricated. After binding streptavidin to biotin on the gold surface, an electrical current was measured for various voltages. A dramatic current increase was observed in the case of biotin-streptavidin binding in comparison with the other two cases: a control group filled with air and a biotin-only binding group. There was a minimal current change in the cases of the biotin-PBST group, the biotin-BSA group, and the biotin-saturated streptavidin group, as compared with the biotin-streptavidin group. At a 0.1 μg/ml concentration of streptavidin (1.5 nM), the current difference before and after the protein binding was amplified by approximately 3000-fold with 17 nm nanogap. Also, the detection sensitivity of the vertical nanogap as the gap size varied was investigated. As the size of biotin-streptavidin binding is the most comparable to 12 nm nanogap, the highest sensitivity was shown in the 12 nm gap device. 7 nm nanogap can be used to detect smaller size of biomolecule than that of biotin streptavidin. This arrayable, two-terminal microdevice could be tested for use on a wide range of other biomolecules. © *2007 American Vacuum Society.* [DOI: 10.1116/1.2713403]

I. INTRODUCTION

Technical advancements in silicon-based microelectronics have been achieved over the past three decades, primarily through the scaling of device dimensions to attain improvements in circuit speed and reduction in size according to Moore's law. An essential key to this progress is miniaturization using microfabrication technologies.[1–3] Applying silicon microfabrication technology for the recognition of protein-ligand binding can produce arrayable microdevices implemented for electrical measurements. Detection time and cost can be drastically reduced due to the full compatibility of fabrication with the semiconductor industry and to label-free processing.

The analysis of protein-ligand binding is a rudimentary tool in the development of the molecular recognition mechanism and the characterization of protein function and novel pharmaceuticals. Thus, various techniques such as fluorescent[4,5] and enzymatic[6,7] approaches have been developed to study protein-ligand binding. Unfortunately, these methods require labeling steps, which are unwieldy and time-consuming procedures. Previous studies have demonstrated a process for electrical detection with labeling.[8] However, this approach may have suffered from the complexity of the labeling process and nanogap formation. As a result, a label-free analysis tool incorporating electrical detection is highly desirable. In this study, a novel approach for the label-free detection of protein-ligand binding by sublithographic vertical nanogap electrodes is reported, including a simple device fabrication process.

For the enhancement of detection sensitivity, a nanogap is required to eliminate an impedance of electrical double layers.[9,10] A nanogap of less than 10 nm is highly desirable in order to retain the high sensitivity necessary to recognize subnanomolar target proteins. However, achieving this size of a nanogap is not an easy task, even with extreme-ultraviolet lithography or electron beam lithography.

Nanogap structures can be classified into two groups: planar and vertical structures. Both electrodes face each other horizontally in the planar nanogap, while they are vertically situated in the vertical nanogap. These structures are shown in Fig. 1. The most critical dimension, the nanogap size, is

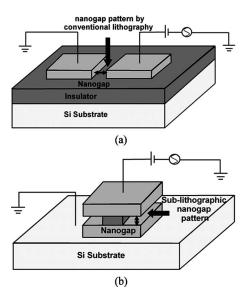[a)]Electronic mail: nobelab@naver.com

FIG. 1. Two types of nanogaps: (a) planar nanogap structure and (b) vertical nanogap structure
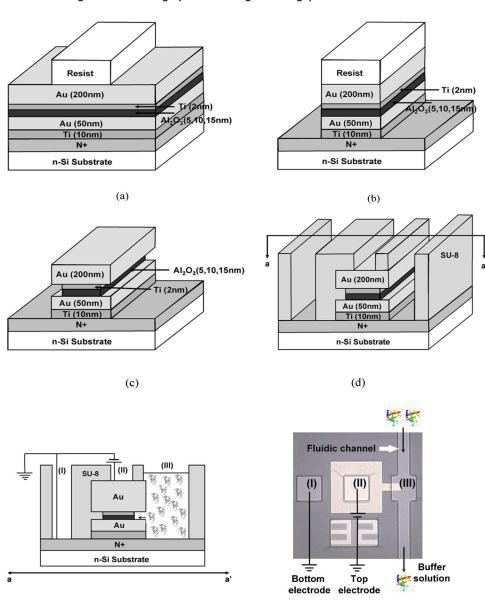
defined by a conventional manner such as photon-, electron-, or ion-beam lithography and subsequent etching. Clearly, there is a resolution limit in defining sub-10-nm features. To overcome the resolution limits, a planar nanogap with spacer lithography using an oxide thin film formed by chemical vapor deposition (CVD) as a sacrificial layer was proposed; however, the design suffered due to the complexity of the process and the narrow process windows for making the nanogaps.[11] Alternatively, a vertical nanogap[12] was demonstrated with polycrystalline electrodes, which can suffer from a parasitic resistive layer caused by polycrystalline depletion effects, relatively low conductivity, and limitations in the types of self-assembled monolayers that are compatible with various biomolecules. Thus, in order to overcome the aforementioned challenges, we propose a novel vertical gold nanogap fabricated using gold electrodes and a sacrificial ultrathin film formed by atomic layer deposition (ALD).

II. FABRICATION AND CHARACTERIZATION

The fabrication process of the novel vertical gold nanogap is shown in Fig. 2. A *n*-type (100) silicon wafer was used as the starting material. The wafer was heavily doped with $POCl_3$ at 1000 °C for eight hours. This heavily doped *n+* region provides Ohmic contact between the bottom electrode and the *n*-type silicon substrate, which serves as a probing pad grounded for electrical measurement. A 10 nm thickness of Ti and a 50 nm thickness of Au were deposited by sputtering. For an atomic-level precision of film thickness in terms of thickness control and uniformity, Al_2O_3 was deposited by atomic layer deposition (ALD) instead of by CVD. Al_2O_3 thin films were grown in a 12×16 in.^{2} large traveling wave ALD reactor with nitrogen as a carrier gas at 250 °C. Trimethylaluminum (TMA) and H_2O were used as precursors of Al and O, respectively. The sequence of pulses for one deposition cycle of Al_2O_3 is TMA $(0.5 \text{ s})/N_2$ $(0.8 \text{ s})/H_2O$ $(1.3 \text{ s})/N_2$ (2.5 s). The growth rate for one

deposition cycle of Al_2O_3 is 0.1 nm at 250 °C. As a result, an extremely thin layer of Al_2O_3 deposited by ALD will determine the nanogap size. The thicknesses of Al_2O_3 were split into three groups, 5, 10, and 15 nm, to investigate how the gap size can affect detection sensitivity via electrical measurement before and after protein-ligand binding. For the formation of top gold electrode, additional layers of Ti (2 nm) and Au (200 nm) were deposited by thermal evaporation. The thin Ti layer is necessary to improve adhesion between the gold and the sacrificial Al_2O_3. Due to this Ti glue layer, the nanogap size is additionally enlarged because Ti is also etched during the Al_2O_3 wet etching in (30:1) buffered HF (BHF). Precise control of Ti thickness is crucial. Then, optical lithography (wavelength=436 nm) with the photoresist (AZ6612K) was used to pattern the electrodes, as shown in Fig. 2(a). Two methods, ion milling with Ar plasma and wet etching with (10:1) KCN and (30:1) buffered HF, were used to etch the gold and titanium. The etched slope is almost the same in both approaches, as shown in Fig. 3. The wet etching method was chosen because the ion milling is basically a physical etch that lacks selectivity between the gold/titanium and the *n+* doped silicon and can cause some damage to the electrode surfaces. Ti and Al_2O_3 were etched by (30:1) buffered HF. As a result, a 7 nm nanogap was fabricated with 5 nm of Al_2O_3 and 2 nm of Ti, as shown in Fig. 4. The etching time governs the lateral nanogap width. The 7 nm nanogap was filled with platinum (Pt), which protected the electrodes from focused ion-beam (FIB) damage during transmission electron microscopy (TEM) sample preparation. The dashed line in Fig. 4(a) represents a boundary between the air gap and the Al_2O_3 layer. The lateral width of by BHF is approximately 40 nm. Then, an SU-8 negative photoresist was used to conduct and confine a buffer solution, including proteins, in the designed area, as shown in Fig. 2(f). Probing pads and other interconnection regions were not exposed to the buffer solution in order to avoid contamination by the buffer solution. Figures 2(e) and 2(f) show probing pads for electrical measurement. The pad denoted as "I" was grounded, and a dc bias was applied to the other pad, denoted by "II." The buffer solution, including proteins, was injected through the fluidic channel made of SU-8 and confined in the region denoted by "III."

III. MEASUREMENTS AND DISCUSSION

As an application of the vertical gold nanogap, it was used for the label-free electrical detection of biotin-streptavidin binding. The construction procedure of the biotin-streptavidin monolayer on the gold surface was[13] as follows. Prior to a self-assembled monolayer (SAM) formation, the vertical gold nanogap was cleaned with pure acetone. The substrates were then washed sequentially with absolute grade ethanol. For SAM formation, the substrate was immersed for more than 2 h in 2 mM of the self-assembly reagent (11-amino-1-undecanethiol, Dojindo) in ethanol solution, followed by a thorough rewashing in ethanol and de-ionized (DI) water. The amine-functionalized substrate was biotinylated by immersion in a solution of sulfo-

FIG. 2. Schematics of fabrication process flow and optical photograph in top view. (a) after thin film deposition and mask, (b) after electrode patterning, (c) after Ti and Al$_2$O$_3$ etch by BHF, (d) after fluidic channel formation with SU-8 to confine buffer solution, (e) cross-sectional view along *a-a′* direction in (d), and (f) optical photograph to show a top view of the fabricated nanogap device.
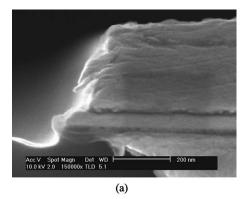
NHS-LC-biotin in a 0.05M bicarbonate buffer at pH of 8.5 for 30 min. To hydrolyze the remaining reactive esters, the substrate was immediately subjected to a solution of sodium bicarbonate buffer at pH of 9.5 for 20 min, followed by washing with DI water. For quantitative analysis, the biotinylated substrates were then immersed in dilute streptavidin solutions (1.5–300 nM) in 10 mM PBST (phosphate buffer saline containing 0.05% Tween-20, pH of 7.4) for 40 min, followed by a thorough washing in PBST and DI water, were dried for 10 min under a stream of nitrogen and were used immediately thereafter. In a vertical gold nanogap that incorporates biotin-streptavidin binding groups, the specific binding between biotin and streptavidin can be detected by an electrical current measurement.

Since we intended to compare our system with different analytes under the same surface condition (i.e., biotin-SAM surface), where the underlying electrode served as a reference with a background signal to the various analytes, we used three experimental groups to investigate the electrical characteristics of biotin-streptavidin binding. The control group was the intact surface group filled with air, the biotin group had a biotin-functionalized surface, and the streptavidin was bound onto the biotin for the biotin-streptavidin group. Figures 5(a) and 5(b) show the *I-V* characteristics at the 17 nm vertical gold nanogap and the concentration of 300 nM streptavidin. The current was measured in the range of 0 to 2 V. As shown in Fig. 5(a), the current increased more dramatically in the biotin-streptavidin binding group than in the other two groups. The current levels were compared among the three groups, as shown in Fig. 5(b) at 1.5 V.

To confirm that the dramatic current change in the biotin-streptavidin binding group did not result from a buffer solution effect, the biotinylated gap surface was analyzed with streptavidin-free PBST buffer solution in the biotin-PBST group. Also, to investigate the specificity of biotin-
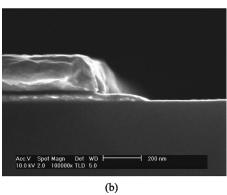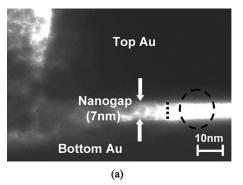
(a)

(b)

FIG. 3. Cross-sectional SEM photographs of the vertical nanogaps: (a) etched by ion milling and (b) etched by (10:1) KCN and (30:1) BHF.

(a)

(b)

FIG. 4. (a) Cross-sectional TEM photographs of 7 nm vertical gold nanogap. Vertical line is an interfacial boundary of Al_2O_3 and air, which is filled with Pt for TEM analysis and (b) close-up view of circle in (a).

streptavidin binding in the vertical gold nanogap, the biotin-BSA (bovine serum albumin) group and the biotin-saturated streptavidin group which consists of *d*-biotin (from Sigma, ~1 nm) and streptavidin were electrically analyzed as well, because the BSA and biotin-saturated streptavidin in the PBST buffer solution are the nonspecific molecules on the biotinylated gap surface. Figure 6(a) shows that there is a little current change in the biotin-PBST, biotin-BSA, and biotin-saturated streptavidin groups, as compared to the biotin-streptavidin group, at 1 V in a 12 nm vertical gold nanogap. Thus, the dramatic current change in the biotin-streptavidin group is not due to a buffer solution effect, but is due to the specificity of biotin-streptavidin binding in the vertical gold nanogap.

The clear conduction mechanism in biotin-streptavidin binding is still not well understood. Additional experiments are underway to clarify the conduction mechanism and charge transfer in biotin-streptavidin binding as the temperature, the gap size, and the concentration of biomolecules are varied. Figure 6(b) shows that the ratio of the current from after (I_p; streptavidin-biotin) to before (I_o; air gap) the binding of streptavidin to biotin in a 17 nm vertical gold nanogap increases as the streptavidin concentration increases from 1.5 to 300 nM. This increase is approximately exponential. Even for 1.5 nM of streptavidin, the current ratio (I_p/I_o) is approximately 10^3. Finally, the gap size affects the detection sensitivity of the vertical gold nanogap, as shown in Fig. 7. Since the length of the sulfo-NHS-LC-biotin is 3–5 nm and that of the streptavidin is about 5 nm, the possibility of bind-
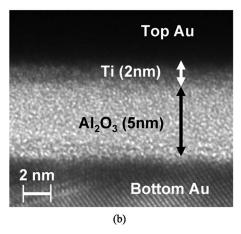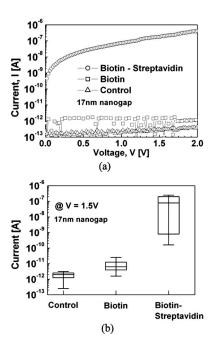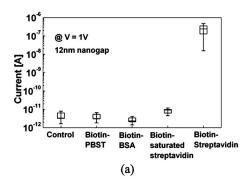

(a)

(b)

FIG. 5. Current-voltage characteristics for three groups: control group, biotin-only group, and biotin-streptavidin binding group with three nanogap device chips, respectively. (a) the biotin-streptavidin binding group shows a dramatic increase of the current from one measurement and (b) the measured current error bar from six data in a single nanogap chip at 1.5 V.
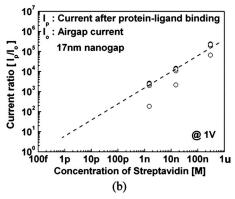
FIG. 6. The ratio of current before and after streptavidin binding with three nanogap device chips as well as current-voltage characteristics for five groups: control group, biotin-PBST group, biotin-BSA group, biotin-saturated streptavidin group, and biotin-streptavidin group with five nanogap device chips. (a) biotin-PBST group, biotin-BSA group, and biotin-saturated streptavidin group show little current change than streptavidin binding group from three to seven data in a single nanogap chip, and (b) as the concentration of streptavidin increases from 1.5 to 300 nM, the ratio of current before (I_o) to after (I_p) streptavidin binding from five data in a single nanogap chip exponentially increases.

ing streptavidin to biotin in a 7 nm gap is small. On the other hand, in 12 and 17 nm gaps, there are suitable spaces to bind the streptavidin to the biotin. Consequently, dramatic current changes occur in the 12 and 17 nm gaps, while the ratio of the current (I_p/I_o) is about 1 in the 7 nm gap. When the gap size decreases from 17 to 12 nm, the ratio of the current
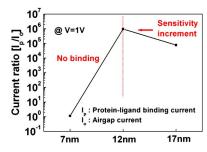

FIG. 7. The ratio of current before and after streptavidin binding from one measurement with three nanogap device chips. As the gap size decreases from 17 to 12 nm, the ratio of current before (I_o) to after (I_p) streptavidin binding increases. There is little current change in the 7 nm gap.

(I_p/I_o) increases as predicted. As a result, the detection sensitivity of the vertical nanogap increases as the gap size decreases.

By changing the sacrificial Al_2O_3 layer thickness, the vertical gold nanogap could be utilized to detect the specific binding of various sizes of protein and ligand. For instance, as a protein-ligand binding application, it is possible that electrical signal activity of phosphorylated peptide induced by kinase can be measured using peptide as a ligand and using kinase as a protein. As another application, vertical nanogap devices could be used in measuring the electrical signal of antigen-antibody interactions. After specific antigen was bound on the nanogap surface, specific molecules of antibody which have specificity of that antigen could be measured electrically.

IV. CONCLUSION

A novel device, the 7 nm sized vertical gold nanogap, was successfully fabricated for the electrical detection of protein-ligand binding without a labeling process. Sublithographic patterns were defined by a sacrificial thin film deposited by ALD. The specificity of detection of biotin-streptavidin binding with the vertical gold nanogap device is demonstrated. 1.5 nM concentrations of streptavidin can be detectable, according to the precise experiments. The vertical gold nanogap device provides a simple and quick analyzing tool to detect protein-ligand binding electrically at a low cost.

[1] R. H. Dennard, F. H. Gaensslen, H. N. Yu, V. L. Rideout, E. Bassous, and A. R. LeBlanc, IEEE J. Solid-State Circuits **9**, 256 (1974).
[2] C. Hu, Semicond. Int. **17**, 105 (1994).
[3] B. Davari, Tech. Dig. - Int. Electron Devices Meet., San Francisco, California, 1996 (IEEE, Piscataway, NJ, 1996), p. 555.
[4] J. Lee, B. G. Gibson, D. J. O'Kane, A. Kohnle, and A. Bacher, Eur. J. Biochem. **210**, 711 (1992).
[5] Y. Chen, J. D. Müller, S. Y. Tetin, J. D. Tyner, and E. Gratton, Biophys. J. **79**, 1074 (2000).
[6] S. Daunert, L. G. Bachas, and M. E. Meyerhoff, Anal. Chim. Acta **208**, 43 (1988).
[7] H. C. Cho, D. J. Lee, S. Y. Kim, J.-H. Kim, I. R. Paeng, and G. S. Cha, Anal. Sci. **15**, 343 (1999).
[8] V. Haguet, D. Martin, L. Marcon, T. Heim, and D. Stievenard, Appl. Phys. Lett. **84**, 1213 (2004).
[9] S. Oh, J. S. Lee, K.-H. Jeong, and L. P. Lee, *Proceedings of the 16th IEEE International MEMS*, Kyoto, Japan, 2003 (IEEE, Piscataway, NJ, 2003), p. 52.
[10] M. Yi, K.-H. Jeong, and L. P. Lee, Biosens. Bioelectron. **20**, 1320 (2005).
[11] Y.-K. Choi, J. S. Lee, J. Zhu, G. A. Somorjai, L. P. Lee, and J. Bokor, J. Vac. Sci. Technol. B **21**, 2951 (2003).
[12] D. D. Carlo, H. Kang, X. Zeng, K.-H. Jeong, and L. P. Lee, *Proceedings of the 12th International Conference on Solid-State Sensors, Actuators and Microsystems*, Boston, MA, 2003 (IEEE, Piscataway, NJ, 2003), p. 1180.
[13] M.-Y. Hong, H. C. Yoon, and H.-S. Kim, Langmuir **19**, 416 (2003).